Design Optimization and Comparative Analysis of Dual-Stator Flux Modulation Machines

Qingsong Wang
Department of Electrical Engineering
The Hong Kong Polytechnic University
Hong Kong, China
q.s.wang@connect.polyu.hk

Shuangxia Niu, *Member, IEEE*
Department of Electrical Engineering
The Hong Kong Polytechnic University
Hong Kong, China
eesxniu@polyu.edu.hk

***Abstract*—This paper proposes three novel dual-stator flux-modulated permanent magnet (DSFMPM) machine concepts, which are particularly suitable for direct-drive applications with the virtue of their high torque density and low operation speed. The dual-stator configuration can help improve the use of inner cavity space, and achieve higher torque density comparing with the single-stator counterparts. Moreover, flux modulation is artfully employed to produce the gear effect, which can further benefit for the torque improvement. According to the PM location, the proposed DSFMPM machines are referred as (i) Stator-PM machine, (ii) Stator-rotor-PM machine, and (iii) Rotor-PM machine. Finite element method coupled with genetic algorithm, namely FEM-GA coupled method, is used to optimal design the proposed DSFMPM machines. Their electromagnetic performances are investigated in detail and quantitatively compared. The results show that the dual-stator topology can well improve the torque capability. Among all the proposed DSFMPM machines, the stator-PM one owns the lowest torque density because it has more short-circuit leakage flux.**

***Keywords*—Dual-stator, flux modulation, genetic algorithm, optimal design.**

I. Introduction

With the potential in alleviating energy crisis and environmental pollution, electric machines are widely used and their developments are accelerating fast[1-4]. In many industrial applications, high-torque low-speed drives are playing significant roles, such as in electric vehicle propulsions [5-7] and wind power generations [8]. Currently, most of these driving systems consist of a high-speed motor with reduction gearbox, which makes the drive systems bulky and inefficient.

Recently, a wealth of magnetic gears (MGs) are proposed [9-11] to replace the mechanical ones in order to alleviate the problems associated with mechanical noise, losses, oil maintenance and so on. The MG can be directly combined with the electric machine, in which the MG has the same function of mechanical gearbox but with lower mechanical noise and free maintenance [12-16]. To further reduce the sizes of the driving systems, various novel machine concepts integrated with magnetic-gearing effect are proposed [17-20], which can achieve high torque density and are suitable for direct-drive applications.

In this paper, three new topologies of dual-stator flux modulated permanent magnet (DSFMPM) machines are proposed, in which the dual-stator concept is incorporated into the FMPM machines. The flux modulating effect integrated with the proposed designs can produce gearing effect, which contribute to the torque improvement. Meanwhile, the dual-stator configuration can help make full use of the inner space of the machines, and the torque capability can be further increased. The working principle of the DSFMPM machines is discussed based on the flux modulating effect. Finite element method coupled with genetic algorithm, which is referred as FEM-GA coupled method, is used to optimal design the proposed DSFMPM machines. Their electromagnetic performances are investigated in detail and compared quantitatively.

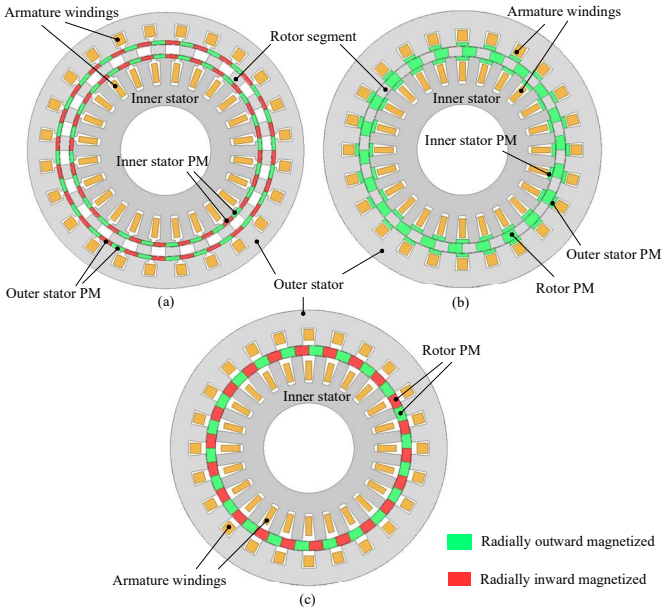

Fig. 1. Configurations of the proposed DSFMPM machines. (a) Machine I. (b) Machine II. (c) Machine III.

II. Constructions and Operating Principle

A. Configurations of the Proposed DSFMPM Machines

The configurations of the proposed DSFMPM machines are shown in Fig. 1. According to the PM location, the

DSFMPM machines can be divided into three novel concepts, which are stator-PM one(Machine I) with all the PMs on the stators, stator-rotor-PM one(Machine II) with the PMs on both the stators and the rotor, and rotor-PM one(Machine III) with all the PMs on the rotor. All the machines have two stators and a middle rotor, the armature windings are housed in the stators.

In machine I, PMs are surface mounted on the stator teeth, and the rotor only have iron segments. The permeance difference between the iron and the air enables the rotor to achieve flux modulating, which is the foundation to achieve magnetic coupling between the PM fields and armature fields. In machine II, the PMs are employed in the slots of the stators and the rotor, and all the PMs magnetized in the same direction, each PM and its adjacent rotor segment/stator tooth form a magnetic pole pair. Bi-directional flux modulating can be achieved since both the rotor and the stators can serve as flux modulator. In machine III, the rotor is yokeless and only consist of PM poles, the stator teeth act as the flux modulator and effective coupling between the PM fields and armature fields can be realized.

B. Operating Principle

The operating principle of the proposed DSFMPM machines is based on the flux modulating effect. Similar to the design principle of magnetic gear and Vernier machine, the stator tooth number N_s, the rotor pole-pair number p_r and the pole-pair number of armature field p_a are governed by:

$$N_s = p_a + p_r \tag{1}$$

The gear ratio G_r is defined as the ratio of rotor pole-pairs to the armature pole-pairs:

$$G_r = \frac{p_r}{p_a} \tag{2}$$

which means the rotating speed of armature field is reduced G_r times, and the rotating speed of the rotor n can be expressed as:

$$n = \left(\frac{60f}{p_a}\right)\frac{1}{G_r} = \frac{60f}{p_r} \tag{3}$$

where f is the frequency of the excitation current.

All the proposed DSFMPM machines have two stators, the winding connection and slot number of the two stators are the same, which means the DSFMPM machines can be regarded as combination of an inner rotor machine and an outer rotor one. For all of the machines being studied in this paper, the selected slot number is 24, the number of stator winding pole-pairs is 2 and the rotor pole-pairs is 22. The rotor pole-pairs is close to the slot number, which is similar to pole-slot combination in Vernier machines and can contribute to the torque improvement[21].

III. Design Optimization

Before comparing the electromagnetic performances of the proposed DSFMPM machines, all the machines are optimal designed using FEM-GA coupled method. The flowchart of the FEM-GA coupled method is shown in Fig. 2. The optimization process contains two stages, which are multi-objective optimization and single-objective optimization. During multi-objective optimization, three objectives are

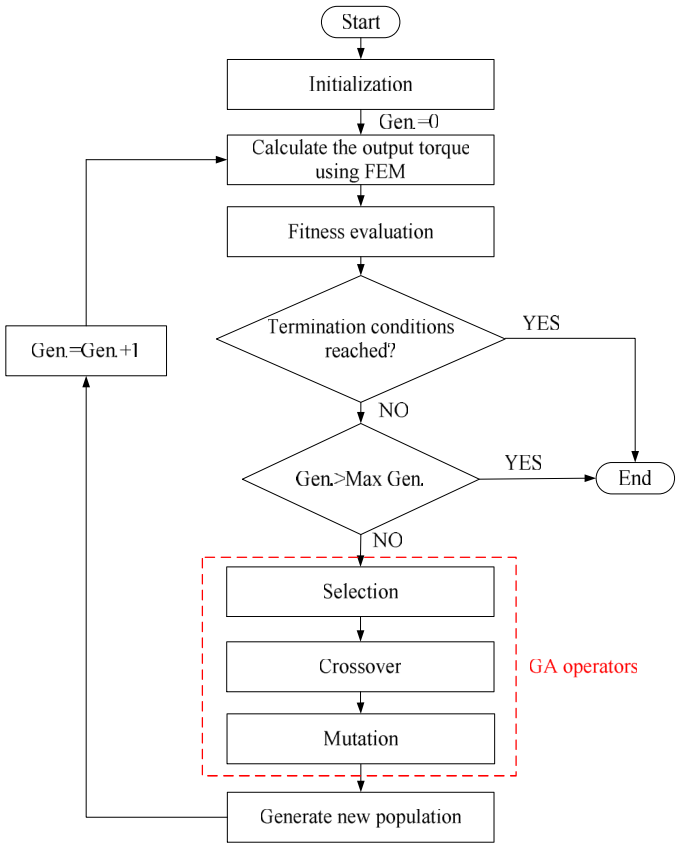

Fig. 2. Flowchart of the FEM-GA coupled method.

TABLE I
PARAMETERS NEED TO BE OPTIMIZED AND THEIR LIMITS

Parameters	Machine I		Machine II		Machine III	
	UV	LV	UV	LV	UV	LV
Outer diameter of inner stator(mm)	170	150	170	150	170	150
Air-gap length(mm)	1.2	0.5	1.2	0.5	1.2	0.5
Rotor thickness(mm)	10	4	10	4	10	4
Tooth width of inner stator(mm)	-	-	11	8	11	8
Tooth width of outer stator(mm)	-	-	16	12	16	12
Thickness of inner stator PM(mm)	6	2	6	2	-	-
Thickness of outer stator PM(mm)	6	2	6	2	-	-
Rotor segment ratio	80%	30%	80%	30%	-	-

investigated, which are the average output torque f_1, the torque ripple ratio f_2 and the efficiency f_3. The optimal design problem is formulated as

$$\min\left\{-f_1(x), f_2(x), -f_3(x)\right\}, \quad x \in F \tag{4}$$

where x is the design parameters, F refers to the constraints of the design parameters, their upper value(UV) and lower value(LV) are given in Table I. f_2 can be expressed in Eq. (5), where T_{max} and T_{min} are the maximum value and minimum value of the steady electromagnetic torque, respectively.

$$f_2(x)=\frac{T_{\max}-T_{\min}}{f_1(x)} \tag{5}$$

The parameterized FE model of these three machines are built using Maxwell package. The output torque may be influenced by many factors, such as pole-slot combination, winding connection and geometrical parameters, etc. In this paper, the pole-slot combination and winding configuration of the DSFMPM machines are the same, the overall diameter and stack length is 245 mm and 50 mm, respectively. The current density is fixed at 8A/mm^2 during optimization.

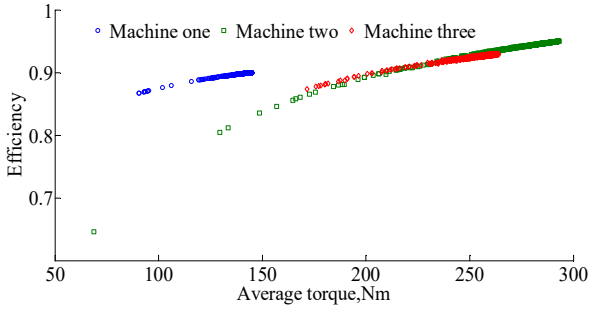

Fig. 3. Relationship between efficiency and average torque.

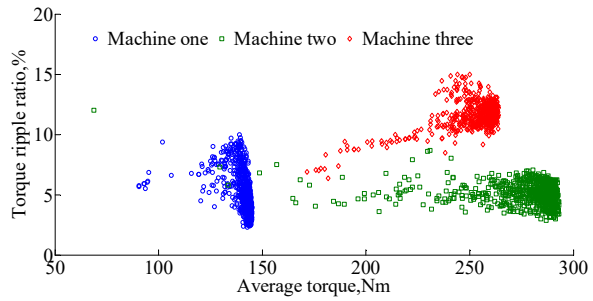

Fig. 4. Relationship between torque ripple ratio and average torque.

Fig. 3 shows the relationship between the efficiency and average torque. It can be observed that the efficiency is positively related with the average torque, when the output torque increases, the efficiency of all the three DSFMPM machines increases accordingly. Therefore, the efficiency and the average output torque can be combined into one single objective during optimization, when the maximum average torque is obtained, the maximum efficiency is achieved as well. Among the three machines studied, machine two can realize the highest average torque and efficiency. Fig. 4 shows the optimization results of the torque ripple ratio and average torque. One can find that the relationship between torque ripple ratio and average torque is almost random. Among the three machines studied, machine three has the largest torque ripple ratio.

After the aforementioned multi-objective optimization, all the three DSFMPM studied in this paper are optimized through single-objective optimization. The objective is to achieve the largest output torque when applied with a fixed current density 8 A/mm^2, the constraint is all the machines should have a torque ripple ratio lower than 12%. The optimal output torque at different iterative number is given in Fig. 5. One can find that machine two and machine three can achieve significantly larger output torque than machine one, the reason behind this is because machine I has much short-circuit leakage flux, which reduces its torque capability. The optimization process can converge within 10 iterations, which shows the effectiveness of the optimization algorithm. The final design parameters after optimization is given in Table II.

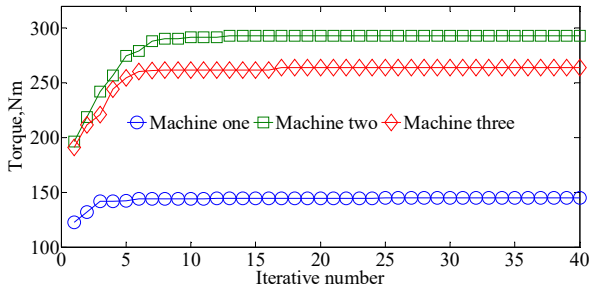

Fig. 5. The optimal output torque at different iterative number.

TABLE II
FINAL DESIGN PARAMETERS

Parameters	Machine I	Machine II	Machine III
Overall diameter(mm)	245		
Stack length(mm)	50		
Outer diameter of inner stator(mm)	164	162	170
Air-gap length(mm)	0.6	0.7	0.6
Rotor thickness(mm)	8	7.5	6
Tooth width of inner stator(mm)	-	9.2	9.8
Tooth width of outer stator(mm)	-	13.8	14.4
Thickness of inner stator PM(mm)	4	3.5	-
Thickness of outer stator PM(mm)	2.5	2.5	-
Rotor segment ratio	50%	45%	-
Armature pole-pairs	2		
Rotor pole-pairs	22		
Stator slot No.	24		
Phase No.	3		
Turns of inner winding	25		
Turns of outer winding	16		
Remanence of NdFeB(T)	1.1		
Relative permeability of NdFeB	1.05		

IV. PERFORMANCE ANALYSIS AND COMPARISON

The electromagnetic performances of the proposed DSFMPM machines are studied and compared in detail. Firstly, the no-load magnetic flux distributions are analyzed and given in Fig. 6. One can find that for all the DSFMPM machines, two pole-pair flux can be obtained in both the inner stator and the outer stator, which can interact with the two pole-pair armature field to generate electromagnetic torque. The machine I has much short-circuit leakage flux, which reduces its power factor and torque capability. The no-load flux linkage waveforms when the DSFMPM machines run at 136 rpm are given in Fig. 7. It can be observed that both the

inner winding and the outer winding in the proposed DSFMPM machines can produce balanced sinusoidal flux linkage waveforms. The corresponding back EMF waveforms are given in Fig. 8, in which we can find that sinusoidal back EMF can be induced in both the inner winding and outer winding as well.

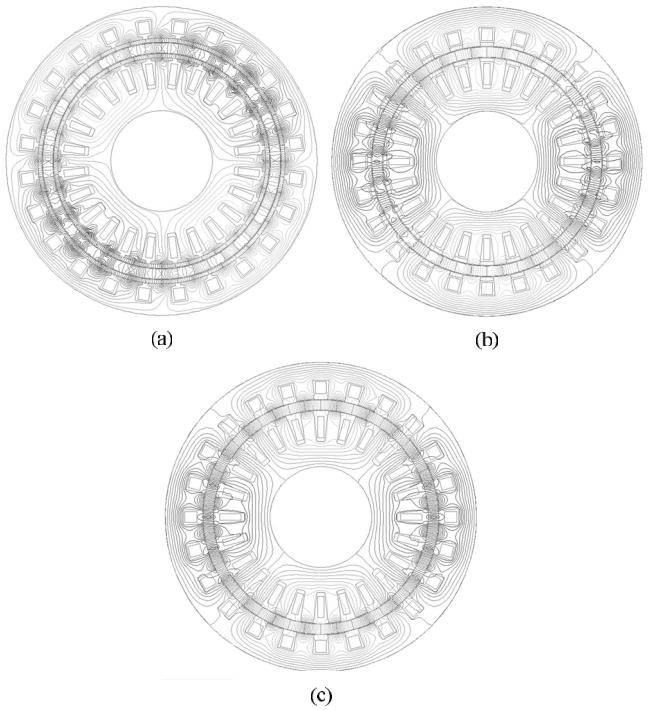

Fig. 6. No-load magnetic flux distributions of the proposed DSFMPM machines. (a) Machine I. (b) Machine II. (c) Machine III.

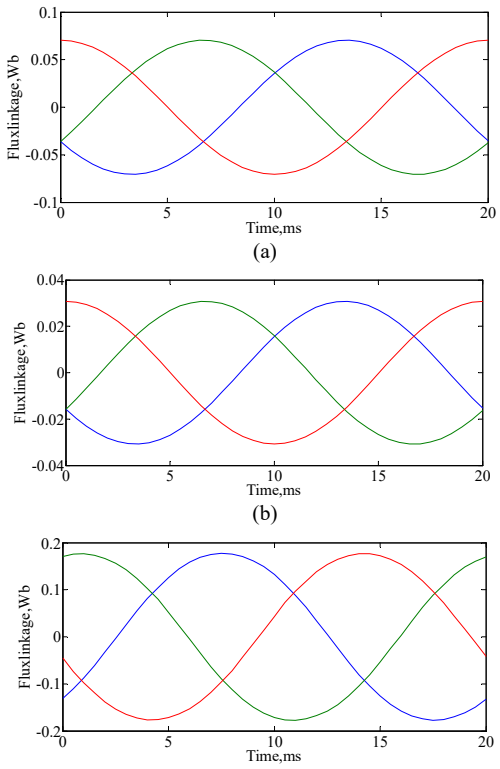

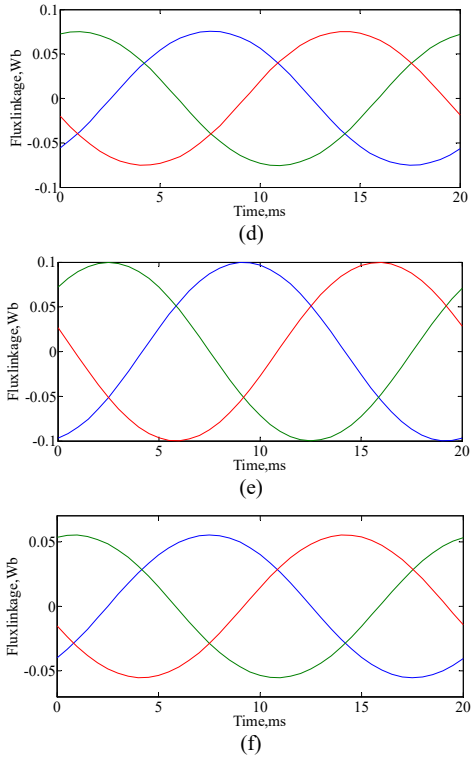

Fig. 7. Flux linkage waveforms. (a) Machine I, inner winding. (b) Machine I, outer winding. (c) Machine II, inner winding. (d) Machine II, outer winding. (e) Machine III, inner winding. (f) Machine III, outer winding.

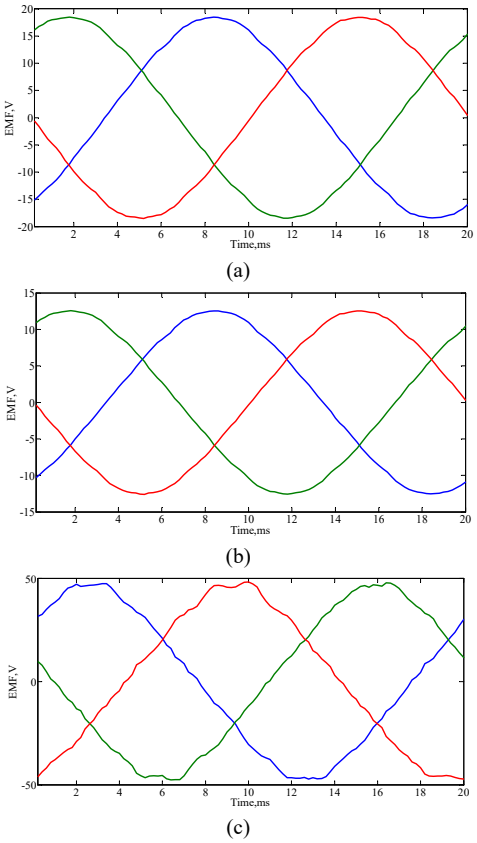

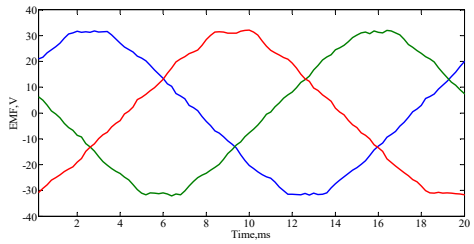

(d)

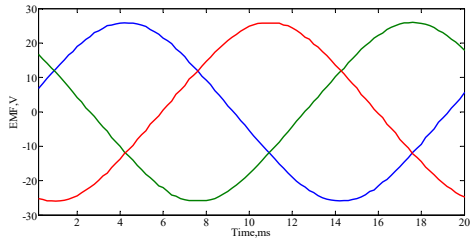

(e)

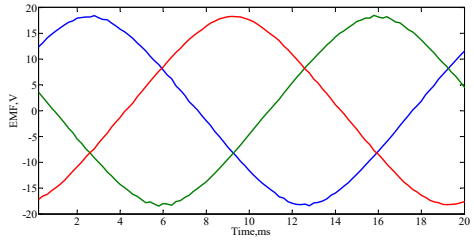

(f)

Fig. 8. No-load back EMF waveforms. (a) Machine I, inner winding. (b) Machine I, outer winding. (c) Machine II, inner winding. (d) Machine II, outer winding. (e) Machine III, inner winding. (f) Machine III, outer winding.

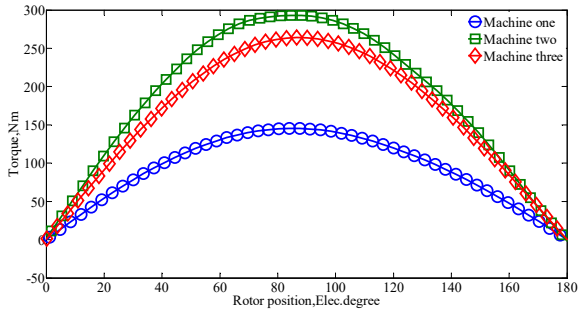

Fig. 9. Stationary torque waveforms.

Fig. 9 shows the stationary torque waveforms when the rotor is locked, and the applied current density is 8A/mm^2. One can find that machine II has the largest output torque, and the output torque of machine I is the smallest. One of the reasons behind this is that machine I has much leakage flux, as can be observed in Fig. 6(a), which reduces its torque capability. The steady state torque waveforms are given in Fig. 10, the torque ripples are 8.8 Nm, 28.9 Nm and 18.7 Nm for machine I, machine II and machine III, respectively, which are only 6% , 10% and 7% of their rated electromagnetic torque. Since the armature currents have big influence on the torque capability, the output torque of the proposed DSFMPM machines when applied with different current density is investigated and shown in Fig. 11. It can be seen that with the increasing of current density, the output torque increases consequently, and the torque-current curves become flat due to magnetic saturation. The magnetic intensity distributions when the current density is 12A/mm^2 are shown in Fig. 12. One can find the machine one and machine two are saturated, which consists with the results shown in Fig. 11.

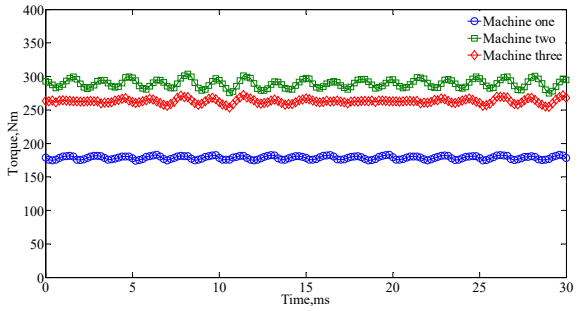

Fig. 10. Steady state torque waveforms.

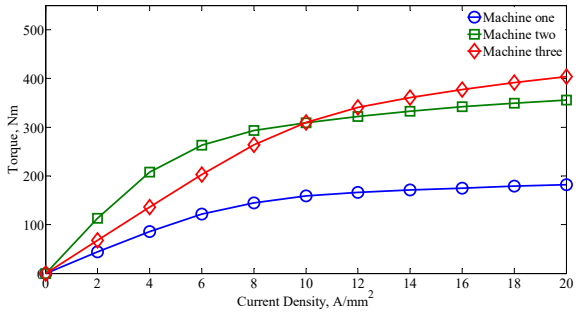

Fig. 11. Torque-current waveforms.

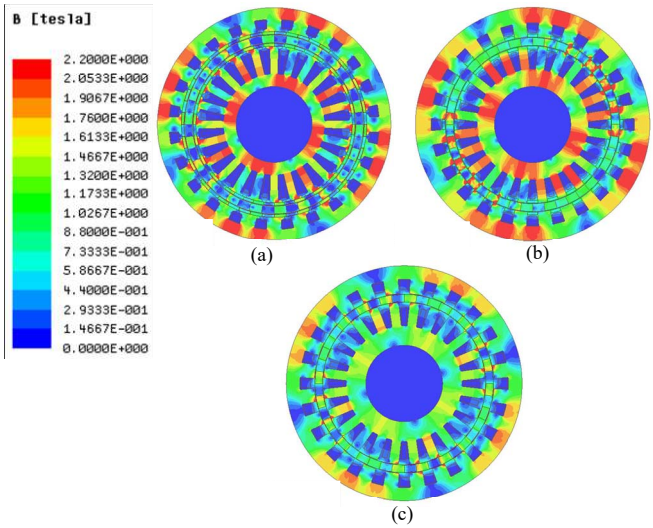

Fig. 12. Magnetic intensity distributions when the current density is 12A/mm^2. (a) Machine I. (b) MachineII. (c) Machine III.

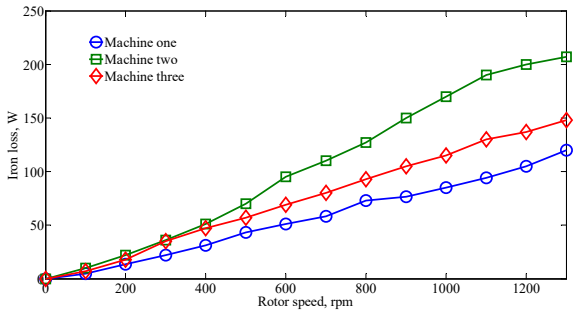

Fig. 13. Iron loss waveforms.

Finally, the iron loss of the proposed DSFMPM machines is studied and given in Fig. 13. One can find that the iron loss is greatly influenced by the rotating speed, because the rotating speed is proportional to the frequency. When the rotating speed increases, the armature frequency increases as well, which will cause the increase of iron loss. Among all the proposed DSFMPM machines, machine II has the highest iron loss. The detail comparison of the electromagnetic performances of the proposed DSFMPM machines is given in Table III.

TABLE III
ELECTROMAGNETIC PERFORMANCES COMPARISON

Items	Machine I	Machine II	Machine III
Rated power (kW)	7.6	15.4	13.8
Rated speed (rpm)	500	500	500
Rated torque (Nm)	145	293	264
Peak torque(Nm)	182	356	404
PM volume(L)	0.17	0.19	0.22
Torque density(kNm/m^3)	77	151	171

V. CONCLUSION

Three novel DSFMPM machines are proposed in this paper, which incorporate the dual-stator concept with flux modulating effect. The dual-stator concept can well improve the utilization of the inner cavity space, and result in higher torque density. Meanwhile, the flux modulating effect can generate gearing effect, which can further increase the torque capability of the proposed machines.

FEM-GA coupled method is used to optimize the designs of the proposed DSFMPM machines, and their electromagnetic performances are investigated in detail and quantitatively compared. The results show that all the proposed DSFMPM machines can achieve high output torque, hence very suitable for direct-drive applications. Compared with machine II and machine III, machine I has higher leakage flux, which reduces its torque capability.

ACKNOWLEDGMENT

This work was supported by research grants (Project PolyU 5388/13E, Project 4-ZZBM, and Project 152130/14E) of the Research Grants Council in the Hong Kong Special Administrative Region, China.

REFERENCES

[1] W. Cao, B. C. Mecrow, G. J. Atkinson, J. W. Bennett, and D. J. Atkinson, "Overview of electric motor technologies used for more electric aircraft (MEA)," *IEEE Trans. Ind. Electron.,* vol. 59, pp. 3523-3531, 2012.

[2] Q. Wang, S. Niu, S. L. Ho, W. Fu, and S. Zuo, "Design and analysis of novel magnetic flux-modulated mnemonic machines," *Electric Power Applications, IET,* vol. 9, pp. 469-477, 2015.

[3] S. L. Ho, Q. Wang, S. Niu, and W. Fu, "A novel magnetic-geared tubular linear machine with halbach permanent-magnet arrays for tidal energy conversion," *IEEE Trans.Magn.*, vol. 51, Nov 2015.

[4] Q. Wang, S. Niu, and X. Luo, "A novel hybrid dual-PM machine excited by AC with DC bias for electric vehicle propulsion," *IEEE Trans. Ind. Electron.,* vol. PP, pp. 1-1, 2017.

[5] D. Dorrell, L. Parsa, and I. Boldea, "Automotive electric motors, generators, and actuator drive systems with reduced or no permanent magnets and innovative design concepts," *IEEE Trans. Ind. Electron.,* vol. 61, pp. 5693-5695, 2014.

[6] K. M. Rahman, N. R. Patel, T. G. Ward, J. M. Nagashima, F. Caricchi, and F. Crescimbini, "Application of direct-drive wheel motor for fuel cell electric and hybrid electric vehicle propulsion system," *IEEE Trans. Ind. Appl.,* vol. 42, pp. 1185-1192, 2006.

[7] Q. Wang and S. Niu, "A novel hybrid-excited flux bidirectional modulated machine for electric vehicle propulsion," in *2016 IEEE Vehicle Power and Propulsion Conference (VPPC)*, 2016, pp. 1-6.

[8] Q. Wang and S. Niu, "Overview of flux-controllable machines: Electrically excited machines, hybrid excited machines and memory machines," *Renewable and Sustainable Energy Reviews,* vol. 68, pp. 475-491, 2017.

[9] V. M. Acharya, J. Z. Bird, and M. Calvin, "A flux focusing axial magnetic gear," *IEEE Trans.Magn.*, vol. 49, pp. 4092-4095, Jul 2013.

[10] K. Atallah and D. Howe, "A novel high-performance magnetic gear," *IEEE Trans.Magn.*, vol. 37, pp. 2844-2846, 2001.

[11] W. Bomela, J. Z. Bird, and V. M. Acharya, "The performance of a transverse flux magnetic gear," *IEEE Trans.Magn.*, vol. 50, Jan 2014.

[12] L. N. Jian, K. T. Chau, and J. Z. Jiang, "A magnetic-geared outer-rotor permanent-magnet brushless machine for wind power generation," *IEEE Trans. Ind. Appl.,* vol. 45, pp. 954-962, May-Jun 2009.

[13] L. Jian, K. T. Chau, and J. Z. Jiang, "A magnetic-geared outer-rotor permanent-magnet brushless machine for wind power generation," *IEEE Trans. Ind. Appl.,* vol. 45, pp. 954-962, 2009.

[14] C. Liu, K. T. Chau, and C. Qiu, "Design and analysis of a new magnetic-geared memory machine," *IEEE Trans. Appl. Supercond.,* vol. 24, pp. 1-5, 2014.

[15] C. Liu, K. T. Chau, J. Zhong, W. Li, and F. Li, "Quantitative comparison of double-stator permanent magnet vernier machines with and without HTS bulks," *IEEE Trans. Appl. Supercond.,* vol. 22, pp. 5202405-5202405, 2012.

[16] Q. Wang, S. Niu, and S. Yang, "Design optimization and comparative study of novel magnetic-geared permanent magnet machines," *IEEE Trans.Magn.*, vol. PP, pp. 1-1, 2017.

[17] L. N. Jian, W. S. Gong, G. Q. Xu, J. N. Liang, and W. X. Zhao, "Integrated magnetic-geared machine with sandwiched armature stator for low-speed large-torque applications," *IEEE Trans.Magn.,*vol. 48, pp. 4184-4187, Nov 2012.

[18] J. G. Bai, P. Zheng, B. Yu, L. M. Cheng, S. K. Zhang, and Z. Y. Liu, "Investigation of a magnetic-field modulated brushless double-rotor machine with the same polarity of PM rotor," *IEEE Trans.Magn.*, vol. 51, Nov 2015.

[19] S. Pakdelian, Y. B. Deshpande, and H. A. Toliyat, "Design of an electric machine integrated with trans-rotary magnetic gear," *IEEE Trans. Energy Convers.,* vol. 30, pp. 1180-1191, Sep 2015.

[20] Q. Wang and S. Niu, "Electromagnetic design and analysis of a novel fault-tolerant flux-modulated memory machine," *Energies,* vol. 8, pp. 8069-8085, 2015.

[21] A. Toba and T. Lipo, "Generic torque-maximizing design methodology of surface permanent-magnet vernier machine," *IEEE Trans. Ind. Appl.,* vol. 36, pp. 1539-1546, 2000.